The Spine Journal 19 (2019) e6–e18

Basic Science

Computed tomography–guided sub–end plate injection of pingyangmycin for a novel rabbit model of slowly progressive disc degeneration

Fuxin Wei, MD, PhD[a], Rui Zhong, MD[a], Ximin Pan, MD[b], Mohammed Khaleel, MD, PhD[c], Aziz Hammoud[d], Zhiyu Zhou, MD, PhD[a], Shaoyu Liu, MD[a,*], Haixing Sun, MD[b], Yajing Zhao, MD[e], Xuenong Zou, MD, PhD[a], Bo Jiang, MD, PhD[b], Wenquan Zhuang, MD, PhD[f], Ningning Chen, MD[a], Yingming Chen, MD[b]

[a] *Department of Spine Surgery, The First Affiliated Hospital and Orthopedic Research Institute of Sun Yat-sen University, No. 58 Zhongshan Er Rd, Guangzhou 510080, People's Republic of China*

[b] *Department of Radiology, The First Affiliated Hospital of Sun Yat-sen University, No. 58 Zhongshan Er Rd, Guangzhou 510080, People's Republic of China*

[c] *Department of Orthopaedic Surgery, The University of Texas Southwestern Medical Center, 5323 Harry Hines Blvd, Dallas, TX 75390, USA*

[d] *The University of Texas Southwestern Medical Center, 5323 Harry Hines Blvd, Dallas, TX 75390, USA*

[e] *The Medical College of Sun Yat-sen University, No. 74 Zhongshan Er Rd, Guangzhou 510080, People's Republic of China*

[f] *Department of Interventional Radiology, The First Affiliated Hospital of Sun Yat-sen University, No. 58 Zhongshan Er Rd, Guangzhou 510080, People's Republic of China*

Received 9 December 2014; revised 6 March 2015; accepted 2 April 2015

Abstract

BACKGROUND CONTEXT: Different animal models are used in disc degenerative disease research by now. To our knowledge, a functional animal model that mimics ischemic and slowly progressive disc degeneration of humans does not exist.

STUDY DESIGN: This is an experimental animal study of disc degeneration.

PURPOSE: The purpose of this study was to establish an ischemic and slowly progressive intervertebral disc (IVD) degeneration model with an injection of pingyangmycin (PYM) into subchondral bone adjacent to the disc, using bone marrow needle guided by computed tomography (CT) scan.

METHODS: The subchondral bone adjacent to the lumbar IVDs (from L3–L4 to L5–L6) of 18 rabbits was randomly injected with 3 mL PYM solution (1.5 mg/mL PYM), 3 mL phosphate-buffered saline (vehicle control), or exteriorized but not injected with anything (sham), with using bone marrow needle guided by CT scan. The degenerative process was investigated by using radiography and magnetic resonance imaging at 1, 3, and 6 months postoperatively, combined with histological scoring, immunohistochemistry, and real-time polymerase chain reaction analysis.

RESULTS: Significant disc space narrowing was observed at 6 months in the discs adjacent to the subchondral bone injected with PYM, compared with the control groups ($p<.05$). The magnetic

FDA device/drug status: Approved (pingyangmycin).

Author disclosures: ***FW:*** Grant: National Natural Science Foundation of China (81401839) (D, Paid directly to institution), Natural Science Foundation of Guangdong (S2013010015775) (C, Paid directly to institution). ***RZ:*** Nothing to disclose. ***XP:*** Nothing to disclose. ***MK:*** Nothing to disclose. ***AH:*** Nothing to disclose. ***ZZ:*** Grant: China Postdoctoral Science Foundation (2013M531876) (C, Paid directly to institution). ***SL:*** Grant: National Natural Science Foundation of China (U1032001) (F, Paid directly to institution). ***HS:*** Nothing to disclose. ***YZ:*** Nothing to disclose. ***XZ:*** Grant: National Natural Science Foundation of China (81272041) (C, Paid directly to institution), National Basic Research Program of China (973 Program, 2012CB619105) (C, Paid directly to institution). ***BJ:*** Nothing to disclose. ***WZ:*** Nothing to disclose. ***NC:*** Nothing to disclose. ***YC:*** Nothing to disclose.

The disclosure key can be found on the Table of Contents and at www.TheSpineJournalOnline.com.

FW, RZ, and XP contributed equally to this work.

∗ Corresponding author. Department of Spine Surgery, The First Affiliated Hospital of Sun Yat-sen University, No. 58 Zhongshan Er Rd, Guangzhou 510080

E-mail address: gzsyliu@tom.com (S. Liu).

https://doi.org/10.1016/j.spinee.2015.04.004

resonance imaging assessment also demonstrated a progressive loss of T2-weighted signal intensity postoperatively. The histological score increased significantly compared with that of the control groups from 3 months to the end point ($p<.05$). The bone tissue area of the end plate increased significantly at the end point, compared with that of the control groups ($p<.05$). The results of molecular analysis showed significant increase of matrix metalloproteinase-3, a disintegrin and metalloproteinase with thrombospondin motif-5, and marked reduction of aggrecan and Type II collagen after 3 months at the messenger RNA levels in the discs of PYM group ($p<.05$). The von Willebrand factor expression of PYM group also showed a significant reduction after 1 month ($p<.05$).

CONCLUSIONS: Percutaneous injection of PYM into the subchondral bone adjacent to the lumbar IVDs of rabbits, using bone marrow needle guided by CT scan, can result in ischemic and slowly progressive disc degeneration model, which mimics the onset of human disc degeneration.

Keywords: Intervertebral disc; Degeneration; Animal model; Computed tomography; Magnetic resonance imaging; Rabbits

Introduction

Low back pain (LBP), one of the most common complaints of individuals, is estimated to affect 60% to 80% of adults at some point in their lives [1]. It is reported that the total annual expenditure attributed to LBP is about $100 billion in the United States [2] and £12 billion in the United Kingdom [3]. Although the pathophysiology inducing LBP is still controversial, intervertebral disc (IVD) degeneration is believed to be a main cause [4,5]. Common findings secondary to degeneration of IVDs include lumbar disc herniation and lumbar stenosis, which may ultimately change the alignment of the lumbar spine, alter disc biomechanics or compress nerve roots, and consequently induce LBP.

The availability of an animal model that consistently reproduces the disease would facilitate investigations of IVD degeneration. There are numerous animal models of disc degeneration that have been developed, including spontaneous degeneration models [6], annulus fibrosus injury models [7], genetic knockout [8], facet removal [9], and chemically induced models [10]. Nonetheless, limited reproducibility, requirement of a high volume of subjects, and requirement of advanced laboratory techniques curtail the widespread use of these models. Additionally, none of these models very effectively simulate the human disease process.

The IVD is the largest avascular structure in the human body. The nutritional pathways supplying the nucleus pulposus work mainly by diffusion through the central portion of the end plate from the bone marrow space and diffusion through the annulus fibrosus from the surrounding vessels [11]. Alteration of the nutrient pathway is considered to be one of the main causes of IVD degeneration [12]. Pingyangmycin (PYM), traditionally a sclerosing agent, has been used as a safe and effective treatment for vascular malformations of the head and neck [13,14]. Intralesionally injected PYM brings the drug into direct contact with the endothelial lining and destroys the endothelial cells (ECs), inducing sclerostenosis of the lumen and resulting in narrowing or occlusion of the vessels [15]. However, whether injection of PYM into subchondral bone adjacent to the IVD could block the nutritional supply of IVD and create a slowly progressive and reproducible model of disc degeneration that theoretically mimics the process of human disc degeneration is still unknown.

To address this question, we injected PYM into the subchondral bone adjacent to the lumbar IVD of rabbits using bone marrow needle, guided by computed tomography (CT), and evaluated the progression of IVD degeneration by histological and genetic studies in combination with the radiographic analysis.

Materials and methods

Animals

Eighteen rabbits (New Zealand Whites, females) with a mean age of 8.22±1.39 (range, 8–9) months old and a mean body weight of 3.23±0.41 (2.68–4.12) kg were used in this study. The study protocol was reviewed and approved by the institutional review board and animal care committee of our university (#2013A-204). Efforts were made to minimize the suffering of animals and the number of animals used.

Study design

In this study, a single concentration of 1.5 mg/mL PYM (Tianjin Taihe Pharmaceutical, Tianjin, People's Republic of China) in phosphate-buffered saline (PBS) was used. The subchondral bone adjacent to the three lumbar IVD segments (from L3–L4 to L5–L6) were randomly injected with 3 mL PYM solution (PYM, n=18), 3 mL PBS alone (vehicle control, n=18), or exteriorized but not injected with anything as a sham surgery (sham, n=18). The process was carried out using CT-guided percutaneous puncture technology.

Experimental surgery

Before surgery, the rabbit was tranquilized by subcutaneous injections of ketamine hydrochloride (10 mg/kg) and midazolam (0.5 mg/kg), followed by midazolam (0.3 mg/kg) and 4 μg fentanyl per hour during operation. Percutaneous needle puncture technology was used to establish this model under fluoroscopic guidance. The rabbits were placed on the operating table in a prone position. The central and the left side of the back were prepared for surgery under sterile surgical conditions. Lateral views of the lumbar spine were obtained using fluoroscopy (Philips Healthcare, Best, The Netherlands). The 17-gauge bone marrow needle was used for puncture in the study. The disc level was selected to determine the placement of the needlepoint, which was 1.5 cm paramedian to the midline. The needle was punctured into the subchondral bone above and below the disc at a distance of 2 mm from the adjacent end plate (Fig. 1A and B) and was directed at an angle of 60° from the coronal plane and parallel to the end plate under fluoroscopic guidance. When the needle tip arrived at the central and anterior parts of the vertebral body, which was measured with the CT scan (Fig. 1C and D), the needle stylus was withdrawn, and the PYM (1.5 mg/mL, 1 mL per hole) solution or PBS was injected into the vertebral body slowly through the cannula using a syringe with the long needle. After injection and removal of the needle, the hole was filled with granular gelatin foam through the cannula to prevent extravasation of PYM. For the sham group, the needle pinpoint touched the rim of the vertebral body but did not puncture into it.

Fig. 1. Fluoroscope and computed tomography (CT)–guided puncture procedure. (A and B) Anterior and lateral views of lumbar spine, confirming the needle was punctured into the subchondral bone above the disc, with 2 mm distance from the adjacent end plate, and (C and D) CT confirmed that the needle tip arrived at the central and anterior parts of the vertebral body.

Before, during, and after operation, the rabbits were given 80 mg/kg of ceftriaxone sodium (Baiyun Pharmaceuticals, Guangzhou, People's Republic of China) subcutaneously. After operation, the rabbits were housed individually with free access to water. All the rabbits tolerated general anesthesia well, and no mortalities from complications caused by anesthesia or infections were found. Weight, food intake, and sleeping habits were recorded.

IVD height measurement

The roentgenograms of the lumbar spine were acquired for all the rabbits by using the Digital Diagnost VM (Philips Healthcare), a multipurpose single-detector digital radiography system. The average IVD height was measured manually by a radiologist (XP) who was blinded to both the injection solution used (PBS/PYM) and the follow-up period. The average IVD and caudal vertebral height were determined by averaging three measurements on the anterior, middle, and posterior side, respectively (Fig. 2).

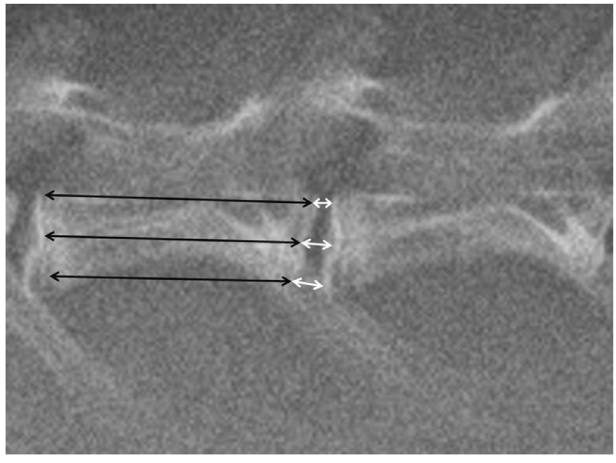

Fig. 2. Radiograph of the lumbar vertebral body and adjacent intervertebral discs of a rhesus monkey. The disc height index was calculated by dividing the average disc height (white arrows) by the average vertebral body height (black arrows).

The measurements were repeated by the same radiologist researcher at the 1-month interval. Then, the average IVD height was divided by the average caudal vertebral height, resulting in a value called the disc height index (DHI) [16], which was used for leveling out interanimal size difference. Changes in the DHI were expressed as loss of %DHI=100 −(DHI measured at follow-up/preoperative DHI×100%) [17].

Magnetic resonance imaging analysis

Each animal underwent magnetic resonance imaging (MRI) on a 1.5-T MR imager (Achieva; Philips Healthcare) in a supine position at the indicated follow-up points. Sagittal sections were made using a T2-weighted spin-echo sequence, a turbo factor 45, and a spine-array coil (repetition time: 2,500 ms, echo time: 100 ms, field of view: 180×180, and section thickness: 3 mm). The disc morphologic changes were graded according to the classification scale described by Pfirrmann et al. [18] by two observers (HS and RZ), respectively, who were blinded to injection solution and follow-up periods. After all the data were collected, the observers together delineated the disc grades for any inconsistent result.

Tissue harvesting

Disc tissues, involving adjacent end plates, were harvested from six rabbits, randomly sacrificed at 1, 3, and 6 months after puncture surgery, by injecting an excess dose of pentobarbital (100 mg/kg, Tianjin Taihe Pharmaceutical, Tianjin, People's Republic of China). All the specimens were dissected into two halves in the sagittal plane. One half was fixed for histological analysis; the cartilage end plates and IVDs from the other half were separated and then snap frozen for messenger RNA (mRNA) analysis.

Histological evaluation and scores

The specimens were fixed with 4% paraformaldehyde for 24 hours at 4°C and then transferred to a sealed vial containing a solution of 70% ethanol and decalcifying agent for 30 days. After being washed with water, the specimens were sequentially dehydrated, split down the midsagittal plane, and embedded in paraffin for histological sectioning. Serial sections were cut in the transverse plane at 6 μm with a microtome (Microtome International, Waldorf, Germany) and then stained with hematoxylin and eosin for cellular constituent and safranin O for proteoglycans [19]. In addition, Masson trichrome staining was used for evaluating collagen fiber orientation.

According to the classification scale described by Masuda et al. [7], the histological changes were qualitatively analyzed by an orthopedic researcher (RZ) who was blinded to the different treatments between groups. The criteria are shown in Table 1. The histological score, ranging from 3 to 9, is the sum of the scores of the three individual parameters, where a score of 1 represents normal and 3 denotes severe degeneration in each category. The analysis was repeated by the same pathologist (YZ) at a 1-month interval.

Table 1
Rabbit disc degeneration Histological Grading Scale*

I Anulus fibrosus
Grade:
1. Normal, pattern of fibrocartilage lamellae without ruptured fibers and without a serpentine appearance anywhere within the annulus
2. Ruptured or serpentine patterned fibers in <30% of the annulus
3. Ruptured or serpentine patterned fibers in >30% of the annulus
II Border between the annulus fibrosus and nucleus pulposus
Grade:
1. Normal
2. Minimally interrupted
3. Moderate/severe interruption
III Cellularity of the nucleus pulposus
Grade:
1. Normal cellularity with large vacuoles in the gelatinous structure of the matrix
2. Slight decrease in the number of cells and fewer vacuoles
3. Moderate/severe decrease (>50%) in the number of cells and no vacuoles

* The classification scale was described by Masuda et al. [7].

Thickness of cartilage end plate

The thickness of the cartilage end plate in the histological samples was measured from the cranial bone end plate to the border between the nucleus pulposus and the cartilage end plate, and the thickness of the bone end plate was measured from the cranial growth end plate to the border between cartilage end plate and the bone end plate. The thickness was determined by an average of three measurements for each image. The ratio of bone tissue area to the whole end plate was also calculated for each sample. The measurements were repeated by the same pathologist at a 1-month interval. Histomorphometric assessment was performed using a digital image analysis system (Nikon Eclipse Ti; Nikon, Tokyo, Japan).

Immunohistochemistry

After being deparaffinized in xylene and rehydrated in a reverse-graded series of ethanol, tissues were prepared for antigen retrieval, quenching of endogenous peroxidase, and blocking of nonspecific binding. They were then incubated overnight at 4°C with either mouse anti-rabbit Type II collagen or aggrecan (1:100; Zhongshan Golden Bridge Biotechnology Co., Ltd., Beijing, People's Republic of China). The remaining procedure was performed in reference to the SA1066 SABC-FITC kit (Boster Corporation, Wuhan, People's Republic of China), and the color (brown) was developed by incubation in DAB (ZSGB-BIO Corporation,

Beijing, People's Republic of China). The sections were counterstained with hematoxylin.

All sections were semiquantitatively analyzed by an orthopedic researcher (RZ), who was blinded to the injection solution, using Image Pro Plus, version 6.0 software, and the integrated optical density (IOD) was measured on the images at ×200 or ×400 magnification. The analysis was repeated by the same pathologist (YZ) at a 1-month interval.

Real-time polymerase chain reaction analysis

Total RNA was extracted from the specimens using Trizol reagent (Ambion, Carlsbad, CA, USA) and purified using the RNeasy Mini Kit (Qiagen, Inc., Duesseldorf, Germany). Reverse transcription was performed at 42°C for 50 minutes using the SuperScript First-Strand Synthesis Kit (Toyobo, Biotech Co., Ltd., Shanghai, People's Republic of China). Aggrecan, Type I collagen (Col1α1), Type II; collagen (Col2α1), matrix metalloproteinase-3 (MMP-3), a disintegrin and metalloproteinase with thrombospondin motifs (ADAMTS)-5, and glyceraldehyde 3-phosphate dehydrogenase (GAPDH) gene expressions of the IVDs were quantified by real-time polymerase chain reaction (PCR) using CFX96 Real-Time System (Bio-Rad, Hercules, CA, USA). The sequences of all the primers used for real-time PCR are shown in Table 2. With a serially diluted complementary DNA sample mixture, a positive standard curve for each primer was obtained for real-time PCR. Quantifications of gene expression for aggrecan, Col1α1, Col2α1, MMP-3, and ADAMTS-5 in the IVDs were calculated using standard curves and normalized to GAPDH in each specimen. To evaluate the number of capillaries in the end plate, the quantification of gene expression for von Willebrand factor (vWF) was also calculated using the same method as described earlier. The mRNA expression was represented as a ratio to the calculation of mRNA in the sham group as the control. The experiments were repeated at least twice for enhanced accuracy.

Statistical analyses

The SPSS, version 16.0, software (SPSS, Inc., Chicago, IL, USA) was used for univariate analysis of variance. The data within groups were analyzed using one-way analysis of variance and Fisher least significant difference test. The paired *t* test was used to compare data between groups. To assess intraobserver reliability, we used the intraclass correlation coefficient for average and single measurement. The agreement of intraclass correlation coefficient and κ statistic was rated as follows: 0 to 0.4, fair agreement; 0.41 to 0.6, moderate agreement; 0.61 to 0.8, substantial agreement; and 0.81 to 1.00, excellent agreement [20]. The data were presented as the mean±standard deviation. Statistical significance was indicated by a p value of less than .05.

Results

No postoperative morbidity or mortality was noted. All animals recovered uneventfully after surgery and quickly resumed normal activities in the cage. None of these animals showed any remarkable change in weight, eating patterns, or sleeping habits.

IVD height

In the sham and vehicle control groups, there were no significant differences in the DHI changes at any time point examined. In contrast, the DHI of the PYM group progressively decreased over time (Fig. 3A−C). However, there were no significant differences compared with that in the sham and vehicle control groups, until the 6-month time point (p=.03, Fig. 3D), at which time, the DHI in the PYM group decreased by 11.9%. The intraclass correlation coefficient was 0.910 for a single measurement with a 95% confidence interval ranging between 0.874 and 0.932 and 0.934 for average

Table 2
The sequence of all the primers used for real-time PCR

Name	GeneBank accession no.		Sequence (5′−3′)
GAPDH	NM_001082253.1	Forward	TGTTTGTGATGGGCGTGAA
		Reverse	CCTCCACAATGCCGAAGT
Aggrecan	XM_002723376.1	Forward	TAAACCCGGTGTGAGAACCG
		Reverse	CCTGGGTGACAATCCAGTCC
Col1α2	NM_001195668.1	Forward	CAATGGTGGCACCCAGTTTG
		Reverse	GGGCCAACGTCCACATAGAA
Col2α1	NM_001195671.1	Forward	GGATAGACCCCAACCAAGGC
		Reverse	GCTGCTCCACCAGTTCTTCT
MMP-3	NM_001082280.1	Forward	GCCAAGAGATGCTGTTGATG
		Reverse	AGGTCTGTGAAGGCGTTGTA
ADAMTS-5	XM_002716775.1	Forward	CACTGTTTCTGGGTGCAG
		Reverse	CTTGACGTTCGGGCCTGA
vWF	XM_008259716.1	Forward	GAATGAGGGGTGTGGCTACC
		Reverse	CACAATCACCTCCCCGTCAA

ADAMTS, a disintegrin and metalloproteinase with thrombospondin motifs; Col1α1, Type I collagen; Col2α1, Type II collagen; GAPDH, glyceraldehyde 3-phosphate dehydrogenase; MMP, matrix metalloproteinases; PCR, polymerase chain reaction; vWF, von Willebrand factor.

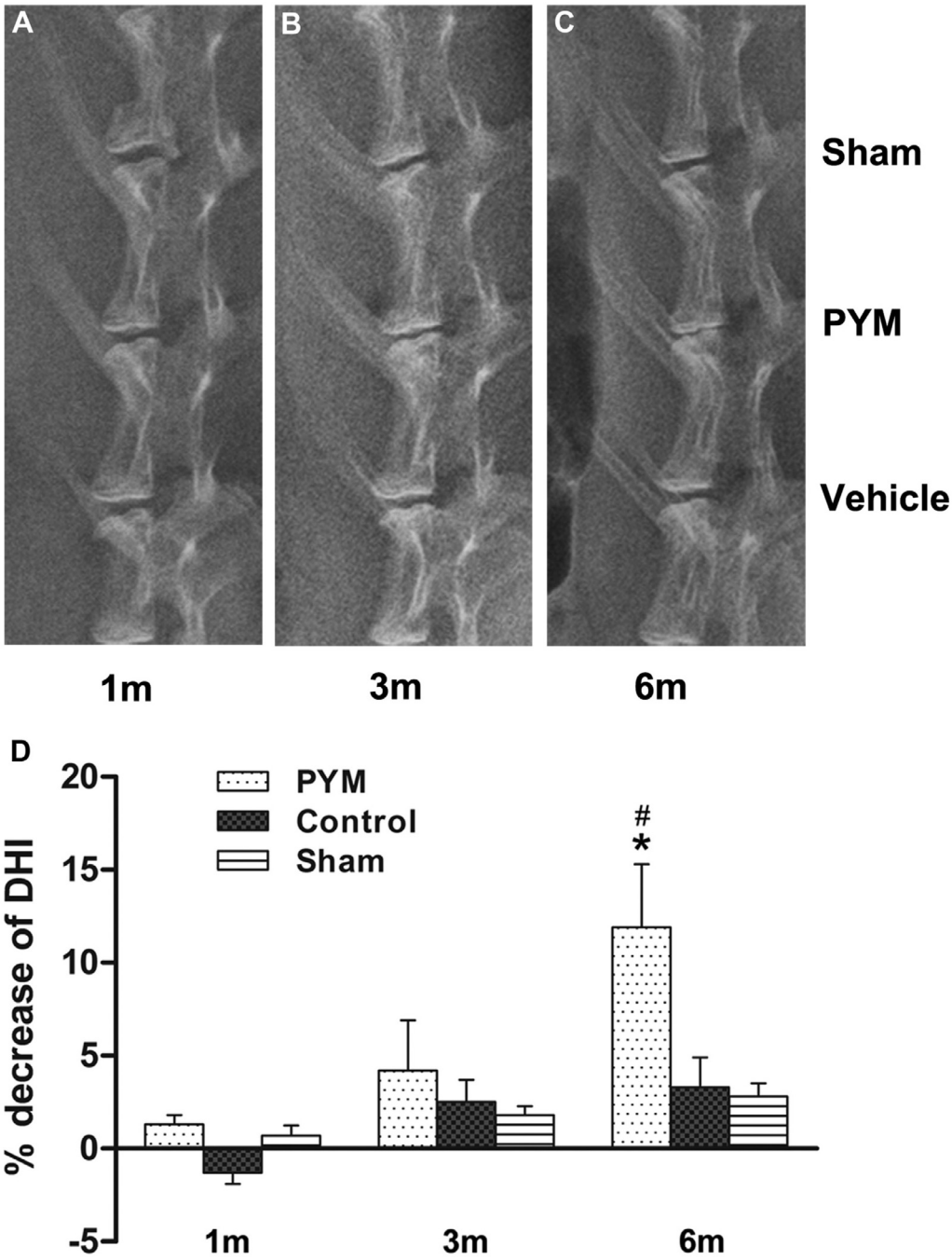

Fig. 3. Representative changes of radiographs at 1, 3, and 6 months postoperatively. (A) No significant changes at the end plate and disc space presented in the disc of pingyangmycin (PYM) group. (B) Mild disc space narrowing presented in the disc of PYM group. (C) The disc height decreased markedly in the PYM group. (D) The mean percent disc height index (DHI) at each time point; # indicated significant difference compared with the sham group, $p<.01$, and * indicated significant difference compared with the vehicle control group, $p<.01$.

measurements with a 95% confidence interval ranging between 0.887 and 0.959, showing strong agreement at two time intervals 1 month apart.

Magnetic resonance imaging

The MR images showed degenerative signs in IVDs injected with PYM (Fig. 4). According to the grading system of Pfirrmann et al. [18], the discs in the PYM group were Grade I at 1 month after operation, demonstrating no disc degeneration (Fig. 4A and D). However, after 3 months, 9 of 12 discs in the PYM group degenerated to Grade II (Fig. 4B and E). At the end of the experiment, four of six discs in the PYM group were Grade III (Fig. 4C and F) and two were Grade II. The discs in the sham and vehicle control groups maintained

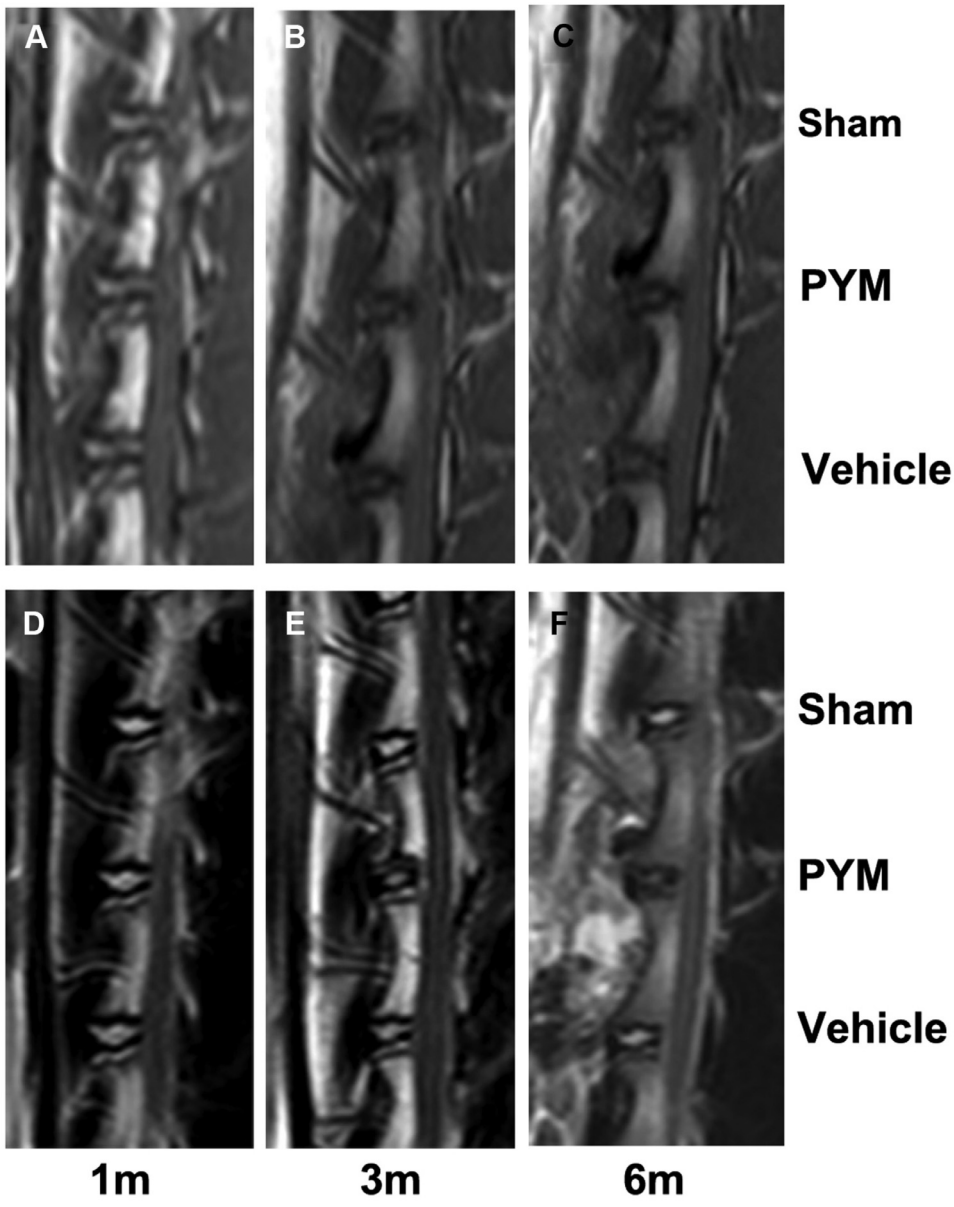

Fig. 4. Representative changes in T1- and T2-weighted magnetic resonance imaging (MRI) scans at 1, 3, and 6 months postoperatively. (A–C) T1-weighted MRI scans at 1, 3, and 6 months postoperatively. (D) Signal intensity of T2-weighted imaging in the disc of pingyangmycin (PYM) group showed no significant change at 1 month postoperatively. (E) Signal intensity of T2-weighted imaging in the PYM-injected disc decreased at 3 months postoperatively. (F) Signal intensity of T2-weighted imaging decreased markedly in the PYM-injected disc at 6 months postoperatively.

the same signal intensity at any time point as that observed preoperatively.

Histological findings and scores

At 1 month after operation, no significant degenerative signs were found in the discs of PYM group, which displayed a round and bloated-looking nucleus pulposus (Fig. 5A) surrounded by an intact annulus fibrosus with a normal pattern of fibrocartilage lamella (Fig. 5B) and consisted of numerous large vacuolated cells with deeply staining proteoglycans (Fig. 5C and D). At 3 months, 8 of 12 discs in the PYM group showed moderate degenerative signs with a grade of 6, in which the nucleus pulposus became elliptic because of the loss of cells with weakly staining proteoglycans (Fig. 5E, F, and H), and the fibrocartilage lamellae showed less organization (Fig. 5F). At 6 months, four of six discs in the PYM group showed more degenerative signs, in which the nucleus pulposus became more elliptic (Fig. 5I), with less cells and proteoglycans (Fig. 5K and L), and the fibrocartilage lamellas became collapsed and wavy (Fig. 5J).

According to the grading system in Table 1, the histological score of the discs in the PYM group

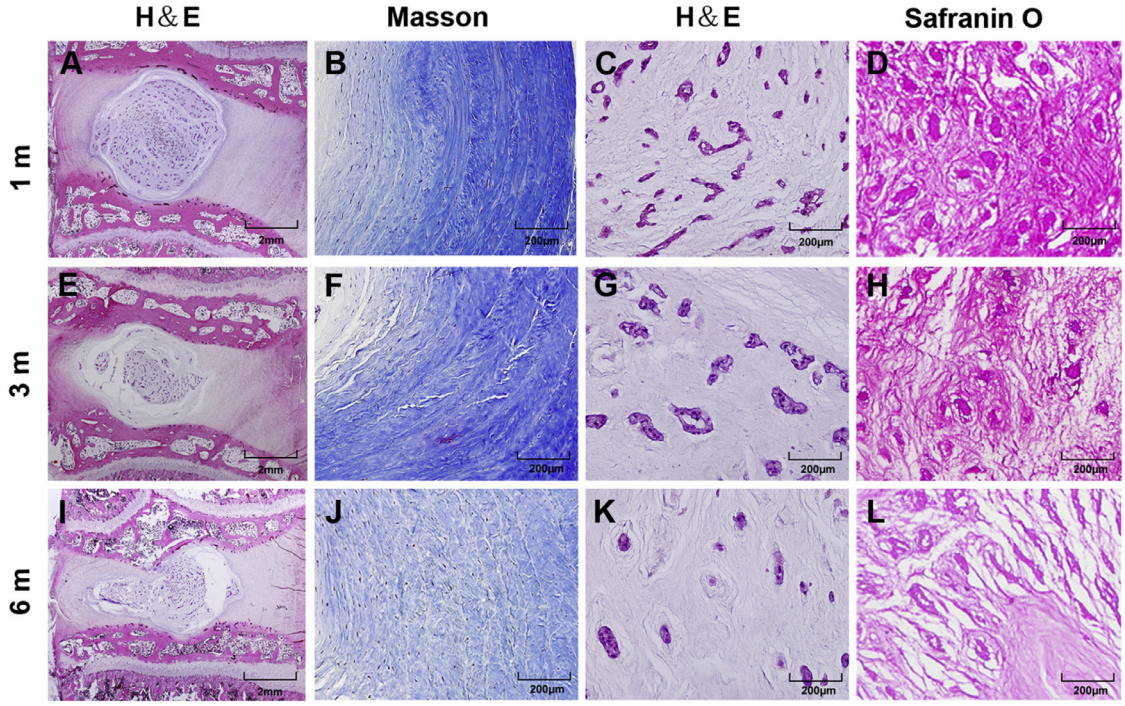

Fig. 5. Typical histomorphological changes seen at 1, 3, and 6 months postoperatively. (A–D) No significant degeneration was observed in the discs of pingyangmycin (PYM) group, which displayed a round and bloated-looking nucleus pulposus surrounded by an intact annulus fibrosus (A) with a normal pattern of fibrocartilage lamellas (B) and consisted of numerous large vacuolated cells with deeply staining proteoglycans (C and D). (E–H) Moderate degenerative signs were observed in the disc of PYM at 3 months, in which the nucleus pulposus became elliptic because of the loss of cells with less stained proteoglycans (E, G, and H) and the fibrocartilage lamellae in the annulus fibrosus showed less organization (F). (I–L) The discs in the PYM group showed severely degenerative signs at 6 months, in which the nucleus pulposus became more elliptic (I), with less cells and proteoglycans (K and L), and the fibrocartilage lamellas became collapsed and wavy (J).

progressively increased over time, reaching significance at the 3-month time point ($p<.05$, Fig. 6, Top), and was significantly higher than that of the sham and vehicle control groups at the 3- and 6-month time points ($p<.05$). The histological scores in the sham and control groups showed no significant differences at any time point ($p<.05$). The intraclass correlation coefficient was 0.895 for a single measurement with a 95% confidence interval ranging between 0.861 and 0.918, showing strong agreement at two time intervals 1 month apart.

Thickness of cartilage end plate

There were no significant differences in the thickness of cartilage end plate between groups until the 6-month time point (Fig. 6, Middle). However, the ratio of the bone tissue area to the whole end plate in the PYM group increased significantly at the 3- and 6-month time points compared with the control and sham groups (Fig. 6, Bottom). The intraclass correlation coefficient was 0.878 for a single measurement with a 95% confidence interval ranging between 0.850 and 0.906 and 0.895 for average measurements with a 95% confidence interval ranging between 0.846 and 0.924, which showed strong agreement.

Immunohistochemistry

Immunohistochemistry assays were performed to evaluate the protein levels of aggrecan in the nucleus pulposus and Type II collagen in the annulus fibrosus. As the cells decreased in the nucleus pulposus of the PYM group, the density of aggrecan staining decreased over time in the PYM group (Fig. 7A–C). A similar trend was also found in the Type II collagen–positive staining of the annulus fibrosus (Fig. 7D and E).

In the PYM group, the average IOD value of Type II collagen in the annulus fibrosus progressively decreased over time. It reached significance at the 6-month time point compared with the 1- and 3-month time points ($p<.05$, Fig. 7A) and was significantly lower than that in the sham and vehicle control groups at the 6-month time point ($p<.05$, Fig. 7G). A similar trend was also found in the IOD value of aggrecan in the nucleus pulpous of the PYM group (Fig. 7D, E, and H). The IOD value of aggrecan in the nucleus pulpous and Type II collagen in the annulus fibrosus showed no significant differences in the sham and

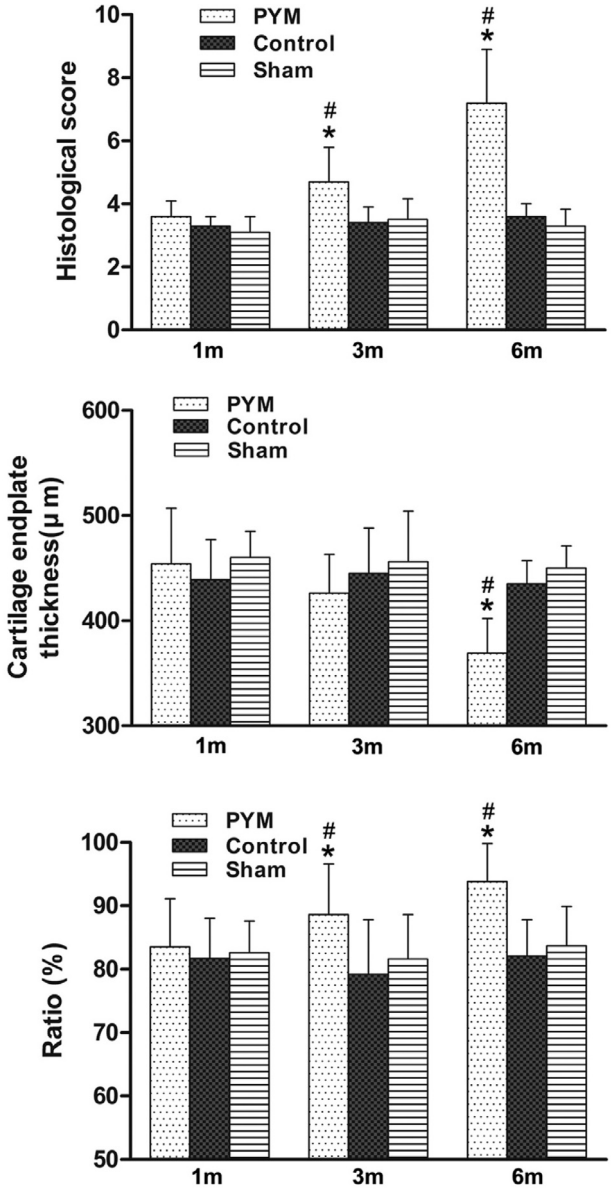

Fig. 6. The histomorphometric assessments of intervertebral discs among the three groups at each time point. (Top) The histological score of the discs between groups at each time point. (Middle) Histomorphometric assessment of cartilage end plate thickness between groups at each time point. (Bottom) Histomorphometric assessment of the ratio of the bone tissue area to the whole end plate between groups at each time point; # indicated significant difference compared with the sham group, $p<.01$, and * indicated significant difference compared with the vehicle control group, $p<.05$.

control groups at any time point ($p>.05$). The intraclass correlation coefficient was 0.882 for the IOD measurements with a 95% confidence interval ranging between 0.841 and 0.915.

Real-time PCR

As compared with the sham and vehicle control groups, the expressions of aggrecan and Col2α1 were significantly lower, and the expressions of MMP-3 and ADAMTS-5 were significantly upregulated in the PYM group from the 3-month time point to the end point ($p<.05$, Fig. 8). There were no significant differences in the expression of Col1α1 between groups ($p>.05$, Fig. 8). The expression of vWF in the PYM group significantly decreased from 1 month to the end point, compared with that of the sham and vehicle control groups ($p<.05$, Fig. 8).

Discussion

In this study, we injected PYM into the subchondral bone adjacent to the lumbar IVDs of rabbits using CT-guided percutaneous puncture technology. We concluded that this could induce slowly progressive disc degeneration, which mimics the onset of degeneration in the human IVD. Histologically, the discs of the PYM group showed degenerative signs from the 3-month time point, at which the nucleus pulposus became elliptic because of the loss of cells with weakly staining proteoglycans, and the fibrocartilage lamellae in the annulus fibrosus showed less organization. The bone tissue area of the end plate in the PYM group also increased significantly at the end point. The MRI assessment demonstrated a progressive loss of T2-weighted signal intensity at the PYM injected discs postoperatively, and disc space narrowing was also observed at 6 months in the PYM group. We also demonstrated that the aggrecan and Type II collagen in the discs of PYM group progressively decreased over time based on the results of immunohistochemistry assays, and the expressions of aggrecan and Col2α1 were significantly lower in the mRNA levels from 3 months to the end point. This suggests an adequate model for spontaneous disc degeneration in the human.

Because the consensus is that the main cause of LBP is typically degenerative disc disease, many studies related to the biological treatment of degenerative disc disease have been reported [21–23]. Thus, it is imperative to establish a reasonable disc degeneration model to evaluate the novel treatment options. Although different methods to induce disc degeneration are currently considered surrogates for middle-aged human beings showing early onset of degenerative disc disease [24], no particular model currently parallels the complex nature of human disc degeneration. The models induced from chemical injuries differ from that normally seen in human IVD degeneration [25]. Direct damage to IVDs, such as annulus fibrosus puncture, have been demonstrated as a suitable method for large animals [7,26]; however, it can induce direct injury and severe damage to IVDs, such as acute nuclear herniation, which is also inconsistent with natural disc degeneration.

To survive and be viable, disc cells require a sufficient nutrient exchange, mostly from the capillaries of the subchondral plate of the vertebral body across the layers of hyaline cartilage that constitute the end plate [12,27]. It has been demonstrated that disorders that affect the blood

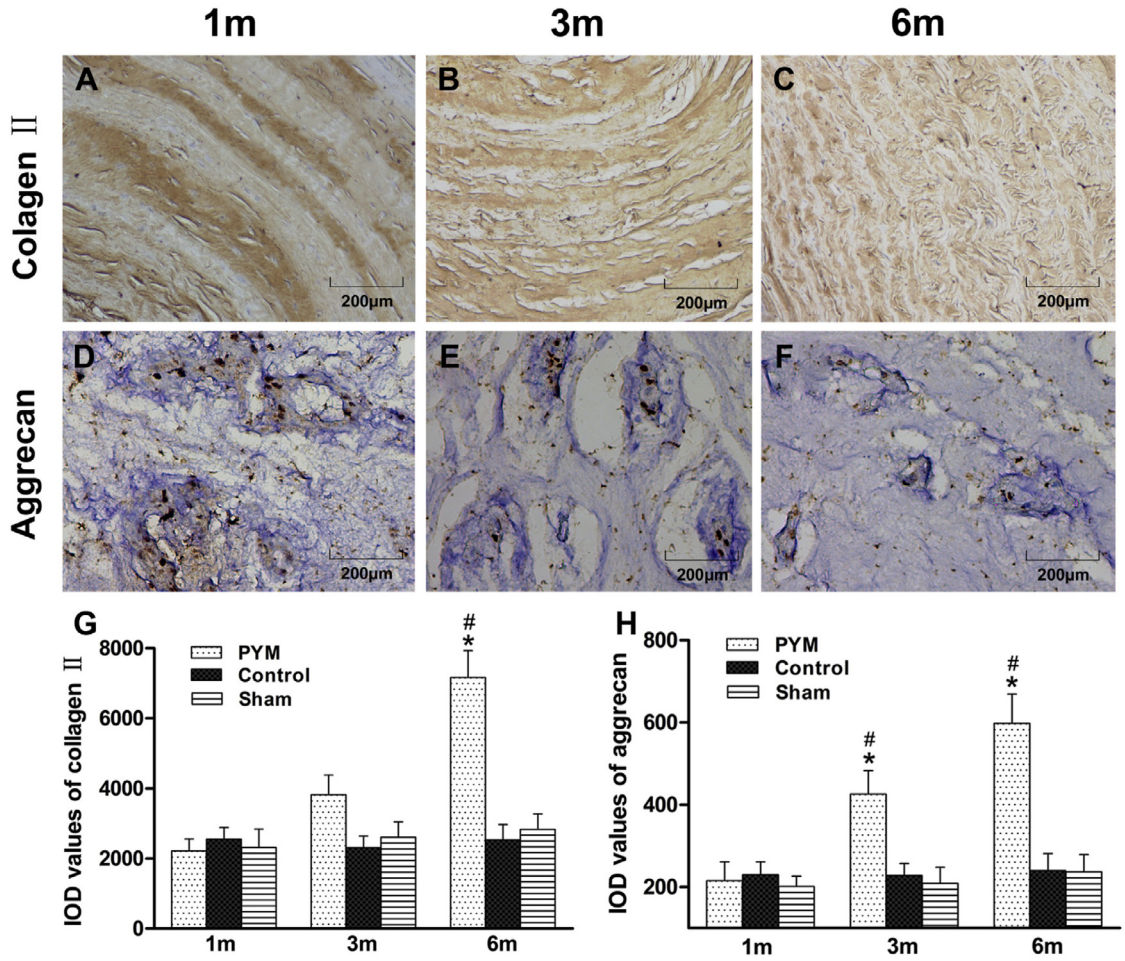

Fig. 7. Immunohistochemistry assay for Type II collagen and aggrecan in the discs of the pingyangmycin (PYM) group. (A−C) Type II collagen−positive staining in the annulus fibrosus decreased over time. (D−F) The density of aggrecan staining also decreased over time in the PYM group. (G) The average integrated optical density (IOD) value of Type II collagen between groups at each time point. (H) The average IOD value of aggrecan between groups at each time point; # indicated significant difference compared with the sham group, p<.01, and * indicated significant difference compared with the vehicle control group, p<.01.

supply to the end plate are significantly associated with disc degeneration and back pain [28,29].

In this study, we injected PYM, which induces a "devascularization effect" [13,14,30], into the subchondral bone adjacent to the IVDs of rabbits to block the nutrient exchange. T2-weighted MR imaging revealed that the disc signal intensity in the PYM group decreased at the 3-month time point after surgery compared with the sham and vehicle groups. The degenerative signs in this model developed slower in comparison with the other animal models, such as needle puncture or chemically induced models, which were reported to degenerate significantly within 2 to 4 weeks [26,31]. However, as disc degeneration develops over several decades in the human, slow development of degeneration in the rabbit is relative. It has been confirmed that the morphologic and MRI changes of IVD degeneration were highly consistent [32]. Pearce et al. [33] also reported that the decreased signal intensity of the disc on T2-weighted MRI scans was significantly related to decreased proteoglycan concentration and progressive degenerative changes of the disc. The histological findings of safranin O staining in this study also confirmed that the proteoglycan content significantly decreased in the nucleus pulposus of the PYM group after surgery, which was consistent with the previous studies showing loss of proteoglycans during the initial phase of disc degeneration [34−36].

Vertebral subchondral bone has been reported to play an important role in maintenance of IVD health [37]. It has been reported that one of the main pathways for nutrients to reach the avascular nucleus pulposus is by diffusion from the blood supply of the vertebral body through the cartilage end plate [12,38,39]. Vertebral subchondral bone malformations, such as Modic changes, calcification, or end plate lesions may affect the nutrient exchange and is specifically associated with degenerative disc disease [40,41]. After injecting PYM into the subchondral bone adjacent to the IVDs, we consistently found that the ratio of the bone tissue area in the end plate of the PYM group increased significantly at 3 months after surgery compared with the control and sham groups. It was proposed that blocking the blood

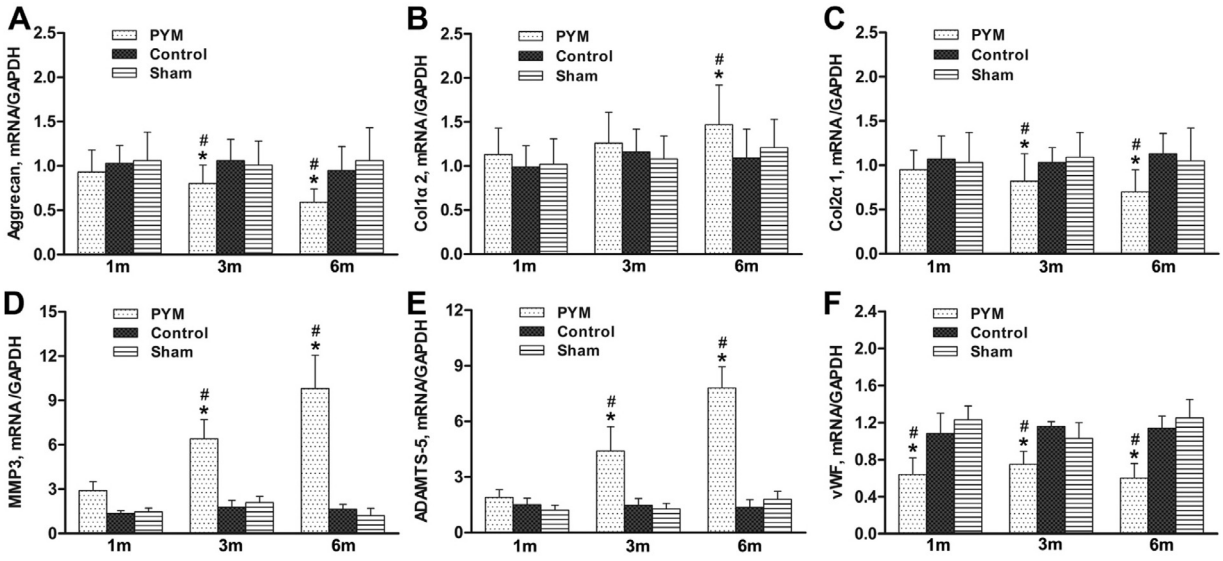

Fig. 8. mRNA expression of aggrecan, Col1α1, Col2α1, MMP-3, ADAMTS-5, and vWF genes at 1, 3, and 6 month postoperatively. This graph showed a marked reduction in aggrecan (A), Col2α1 (C), and significant increase of MMP-3 (D) and ADAMTS-5 (E) in the PYM injected discs after 3 months, up-regulation of Col1α1 after 6 months (B), and significant reduction of vWF expressions after 1 month at the mRNA level (F), compared with the control groups. # Indicated significant difference compared with the Sham group, $p<.01$; $*$ Indicated significant difference compared with the Vehicle control group, $p<.01$.

supply of the subchondral bone to the end plate might lead to calcification of the end plate, which contributed to poor nutrient diffusion and supply into the nucleus that in turn induced disc degeneration [42].

A concern arises that the IVD degeneration might be because of a direct chemical effect of the PYM injected. In the preliminary experiment of this study, when the PYM was injected into the subchondral bone adjacent to the IVDs of rabbits, the X-ray angiography and digital subtraction angiography showed that the contrast medium concentrated in the vertebral body and did not infiltrated into the IVD directly (see Supplementary Fig. 1). In addition, the halftime of PYM is just 1.5 hours. So, we think that the IVD degeneration was mainly induced by the ischemic effect of PYM other than the direct chemical effect. This was also supported by the results of real-time PCR which showed that the expression of vWF that commonly used as an marker for capillary ECs [43,44] significantly decreased in the PYM group compared with that in the sham and vehicle control groups. This might be caused by PYM injection, which could destroy the ECs.

The degenerative changes in the IVDs, such as changes in composition of extracellular matrix, loss of disc cells, proteoglycan, and water content, have been suggested to be the consequence of an upregulation of catabolic MMPs and two major aggrecanases, ADAMTS-4 and -5 [45,46]. Consistent with the previous reports [45,46], we found that mRNA expression of MMP-3 and ADAMTS-5 were significantly increased in the discs of PYM groups compared with the sham and vehicle control groups. It has been reported that disturbance of nutrient transport in IVDs could result in high level of lactic acid and acid pH values [47,48], which might contribute to the overexpression of various proteolytic enzymes and other catabolic agents, such as MMPs. The reasons for the increased MMPs and ADAMTS family in the IVD cells deserve detailed study.

In human discs, the notochordal cells are lost during adolescence, which is also when discs begin to show degenerative signs [49]. Although the cell population significantly decreased in the nucleus pulposus of this degenerative model, notochordal cells are still observed in the rabbit disc at the ages used in this study. This limits relevance to humans; however, the changes in the degenerative model in this study confirmed that PYM injected into the subchondral bone adjacent to the IVD could induce early disc degeneration, which showed some similar characteristic features to the complex processes of disc degeneration in humans, such as disc height loss, significant decrease of cell population, aggrecan, and Type II collagen.

However, this study has some further limitations. One limitation is that there are some biomechanical and anatomic differences between the spine of the rabbits and that of the human. It has been reported that mechanical loading could impair diffusion of nutrients entering the disc and quite possibly accelerate disc degeneration [50]; thus, load bearing may be a significant difference in the degenerative process of this rabbit model and that seen in humans. A further limitation was that we did not perform biomechanical evaluation, such as hydrostatic pressure in the degenerative discs; therefore, additional studies are warranted to evaluate the mechanism and characteristics of disc degeneration induced by PYM.

Conclusions

This present study demonstrates that the injection of PYM into the subchondral bone adjacent to the lumbar IVDs of rabbits can induce ischemic and slowly progressive disc degeneration, which mimics the onset of human disc degeneration. This degeneration model is suitable for disc degeneration and regeneration studies. Further studies to fully establish this model, however, are needed.

Acknowledgements

This study was supported by National Natural Science Foundation of China (81401839, 81272041, and U1032001), National Basic Research Program of China (973 Program, 2012CB619105), China Postdoctoral Science Foundation (2013M531876), and Natural Science Foundation of Guangdong (S2013010015775). The authors thank Shiqian Yu, Sannv Zheng, and Xuejun Dai for their technical and surgical assistance. The authors also thank Steffen Ringgaard for technical assistance of T1ρ imaging.

Supplementary data

Supplementary data related to this article can be found at http://dx.doi.org/10.1016/j.spinee.2015.04.004.

References

[1] Waddell G, Burton AK. Occupational health guidelines for the management of low back pain at work: evidence review. Occup Med 2001;51:124–35.
[2] Battié MC, Videman T. Lumbar disc degeneration: epidemiology and genetics. J Bone Joint Surg Am 2006;88:S3–9.
[3] Dagenais S, Caro J, Haldeman S. A systematic review of low back pain cost of illness studies in the United States and internationally. Spine J 2008;8:8–20.
[4] Deyo RA, Weinstein JN. Low back pain. N Engl J Med 2001;344:363.
[5] Andersson GB. Epidemiological features of chronic low back pain. Lancet 1999;354:581–5.
[6] Bergknut N, Rutges JP, Kranenburg HJ, Smolders LA, Hagman R, Smidt HJ, et al. The dog as an animal model for intervertebral disc degeneration? Spine 2012;37:351–8.
[7] Masuda K, Aota Y, Muehleman C, Imai Y, Okuma M, Thonar EJ, et al. A novel rabbit model of mild, reproducible disc degeneration by an annulus needle puncture: correlation between the degree of disc injury and radiological and histological appearances of disc degeneration. Spine 2005;30:5–14.
[8] Li B, Zheng XF, Ni BB, Yang YH, Jiang SD, Lu H, et al. Reduced expression of insulin-like growth factor 1 receptor leads to accelerated intervertebral disc degeneration in mice. Int J Immunopathol Pharmacol 2013;26:337–47.
[9] Kaigle AM, Holm SH, Hansson TH. Experimental instability in the lumbar spine. Spine 1995;20:421–30.
[10] Xia M, Zhu Y. Fibronectin fragment activation of ERK increasing integrin α5 and β1 subunit expression to degenerate nucleus pulposus cells. J Orthop Res 2011;29:556–61.
[11] Haschtmann D, Stoyanov JV, Gédet P, Ferguson SJ. Vertebral endplate trauma induces disc cell apoptosis and promotes organ degeneration in vitro. Eur Spine J 2008;17:289–99.
[12] Grunhagen T, Wilde G, Soukane DM, Shirazi-Adl SA, Urban JP. Nutrient supply and intervertebral disc metabolism. J Bone Joint Surg Am 2006;88:30–5.
[13] Yue H, Qian J, Elner VM, Guo J, Yuan YF, Zhang R, et al. Treatment of orbital vascular malformations with intralesional injection of pingyangmycin. Br J Ophthalmol 2013;97:739–45.
[14] Zheng JW, Yang XJ, Wang YA, He Y, Ye WM, Zhang ZY. Intralesional injection of pingyangmycin for vascular malformations in oral and maxillofacial regions: an evaluation of 297 consecutive patients. Oral Oncol 2009;45:872–6.
[15] Wang C, Liu J, Pan W, Wang X, Gao Q, Hou S. Pingyangmycin loaded bovine serum albumin microspheres for chemoembolization therapy—in vitro and in vivo studies. Int J Pharm 2008;351:219–26.
[16] Lü DS, Shono Y, Oda I, Abumi K, Kaneda K. Effects of chondroitinase ABC and chymopapain on spinal motion segment biomechanics. An in vivo biomechanical, radiologic, and histologic canine study. Spine 1997;22:1828–35.
[17] Hoogendoorn RJ, Wuisman PI, Smit TH, Everts VE, Helder MN. Experimental intervertebral disc degeneration induced by chondroitinase ABC in the goat. Spine 2007;32:1816–25.
[18] Pfirrmann CW, Metzdorf A, Zanetti M, Hodler J, Boos N. Magnetic resonance classification of lumbar intervertebral disc degeneration. Spine 2001;26:1873–8.
[19] Rosenberg L. Chemical basis for the histological use of safranin O in the study of articular cartilage. J Bone Joint Surg Am 1997;53:69–82.
[20] Shrout PE. Measurement reliability and agreement in psychiatry. Stat Methods Med Res 1998;7:301–17.
[21] Wang SZ, Rui YF, Tan Q, Wang C. Enhancing intervertebral disc repair and regeneration through biology: platelet-rich plasma as an alternative strategy. Arthritis Res Ther 2013;15:220.
[22] Benneker LM, Andersson G, Iatridis JC, Sakai D, Härtl R, Ito K, et al. Cell therapy for intervertebral disc repair: advancing cell therapy from bench to clinics. Eur Cell Mater 2014;27:5–11.
[23] Ren S, Liu Y, Ma J, Liu Y, Diao Z, Yang D, et al. Treatment of rabbit intervertebral disc degeneration with co-transfection by adeno-associated virus-mediated SOX9 and osteogenic protein-1 double genes in vivo. Int J Mol Med 2013;32:1063–8.
[24] Singh K, Masuda K, An HS. Animal models for human disc degeneration. Spine J 2005;5:267S–79S.
[25] Chan SC, Bürki A, Bonél HM, Benneker LM, Gantenbein-Ritter B. Papain-induced in vitro disc degeneration model for the study of injectable nucleus pulposus therapy. Spine J 2013;13:273–83.
[26] Xi Y, Kong J, Liu Y, Wang Z, Ren S, Diao Z, et al. Minimally invasive induction of an early lumbar disc degeneration model in rhesus monkeys. Spine 2013;38:E579–86.
[27] Urban JP, Holm S, Maroudas A, Nachemson A. Nutrition of the intervertebral disc: effect of fluid flow on solute transport. Clin Orthop Relat Res 1982: 296–302.
[28] Urban MR, Fairbank JC, Etherington PJ, Loh FRCA L, Winlove CP, Urban JP. Electrochemical measurement of transport into scoliotic intervertebral discs in vivo using nitrous oxide as a tracer. Spine 2001;26:984–90.
[29] Bibby SR, Fairbank JC, Urban MR, Urban JP. Cell viability in scoliotic discs in relation to disc deformity and nutrient levels. Spine 2002;27:2220–8.
[30] Chen Y, Li Y, Zhu Q, Zeng Q, Zhao J, He X, et al. Fluoroscopic intralesional injection with pingyangmycin lipiodol emulsion for the treatment of orbital venous malformations. AJR Am J Roentgenol 2008;190:966–71.
[31] Norcross JP, Lester GE, Weinhold P, Dahners LE. An in vivo model of degenerative disc disease. J Orthop Res 2003;21:183–8.
[32] Sobajima S, Kompel JF, Kim JS, Wallach CJ, Robertson DD, Vogt MT, et al. A slowly progressive and reproducible animal model of intervertebral disc degeneration characterized by MRI, X-ray, and histology. Spine 2005;30:15–24.

[33] Pearce RH, Thompson JP, Bebault GM, Flak B. Magnetic resonance imaging reflects the chemical changes of aging degeneration in the human intervertebral disc. J Rheumatol Suppl 1991;27:42–3.
[34] Antoniou J, Steffen T, Nelson F, Winterbottom N, Hollander AP, Poole RA, et al. The human lumbar intervertebral disc: evidence for changes in the biosynthesis and denaturation of the extracellular matrix with growth, maturation, ageing, and degeneration. J Clin Invest 1996;98:996–1003.
[35] Anderson DG, Tannoury C. Molecular pathogenic factors in symptomatic disc degeneration. Spine J 2005;5:260S–6S.
[36] Leung VY, Chan D, Cheung KM. Regeneration of intervertebral disc by mesenchymal stem cells: potentials, limitations, and future direction. Eur Spine J 2006;15:S406–13.
[37] Roberts S, Urban JP, Evans H, Eisenstein SM. Transport properties of the human cartilage endplate in relation to its composition and calcification. Spine 1996;21:415–20.
[38] Brodin H. Paths of nutrition in articular cartilage and intervertebral discs. Acta Orthop Scand 1955;24:177–83.
[39] Urban JP, Holm S, Maroudas A. Diffusion of small solutes into the intervertebral disc: as in vivo study. Biorheology 1978;15:203–21.
[40] Nguyen C, Poiraudeau S, Rannou F. Vertebral subchondral bone. Osteoporos Int 2012;23:S857–60.
[41] Wu Y, Cisewski S, Sachs BL, Yao H. Effect of cartilage endplate on cell based disc regeneration: a finite element analysis. Mol Cell Biomech 2013;10:159–82.
[42] Nachemson A, Lewin T, Maroudas A, Freeman MA. In vitro diffusion of dye through the end-plates and the annulus fibrosus of human lumbar inter-vertebral discs. Acta Orthop Scand 1970;41:589–607.
[43] Pusztaszeri MP, Seelentag W, Bosman FT. Immunohistochemical expression of endothelial markers CD31, CD34, von Willebrand factor, and Fli-1 in normal human tissues. J Histochem Cytochem 2006;54:385–95.
[44] Scheja A, Akesson A, Niewierowicz I, Wallin L, Wildt M, Wollheim FA. Computer based quantitative analysis of capillary abnormalities in systemic sclerosis and its relation to plasma concentration of von Willebrand factor. Ann Rheum Dis 1996;55:52–6.
[45] Weiler C, Nerlich AG, Zipperer J, Bachmeier BE, Boos N. SSE Award Competition in Basic Science: expression of major matrix metalloproteinases is associated with intervertebral disc degradation and resorption. Eur Spine J 2002;11:308–20.
[46] Millward-Sadler SJ, Costello PW, Freemont AJ, Hoyland JA. Regulation of catabolic gene expression in normal and degenerate human intervertebral disc cells: implications for the pathogenesis of intervertebral disc degeneration. Arthritis Res Ther 2009;11:R65.
[47] Kitano T, Zerwekh JE, Usui Y, Edwards ML, Flicker PL, Mooney V. Biochemical changes associated with the symptomatic human intervertebral disk. Clin Orthop Relat Res 1993: 372–7.
[48] Diamant B, Karlsson J, Nachemson A. Correlation between lactate levels and pH in discs of patients with lumbar rhizopathies. Experientia 1968;24:1195–6.
[49] Hirata H, Yurube T, Kakutani K, Maeno K, Takada T, Yamamoto J, et al. A rat tail temporary static compression model reproduces different stages of intervertebral disc degeneration with decreased notochordal cell phenotype. J Orthop Res 2014;32:455–63.
[50] Arun R, Freeman BJ, Scammell BE, McNally DS, Cox E, Gowland P. ISSLS Prize Winner: what influence does sustained mechanical load have on diffusion in the human intervertebral disc? An in vivo study using serial postcontrast magnetic resonance imaging. Spine 2009;34:2324–37.